CHAPTER IV
RESULTS AND DISCUSSION

4.1 Preliminary Result

4.1.1 Blank Test

It was found that, when helium was pressurized into the system, the helium leakage was very small as shown in Figure 4.1. With the initial helium pressure at 2000 psig, the pressure drop is only 1.72 psig after 12 hr. Compared with the hydrogen leakage, the pressure drop is higher but still not significant; for example, the pressure drop for hydrogen is 5.23 psig at room temperature after 12 hr. The system was adjusted to minimize the leakage so that any data correction from the hydrogen absorption experiment in section 4.3 is not necessary.

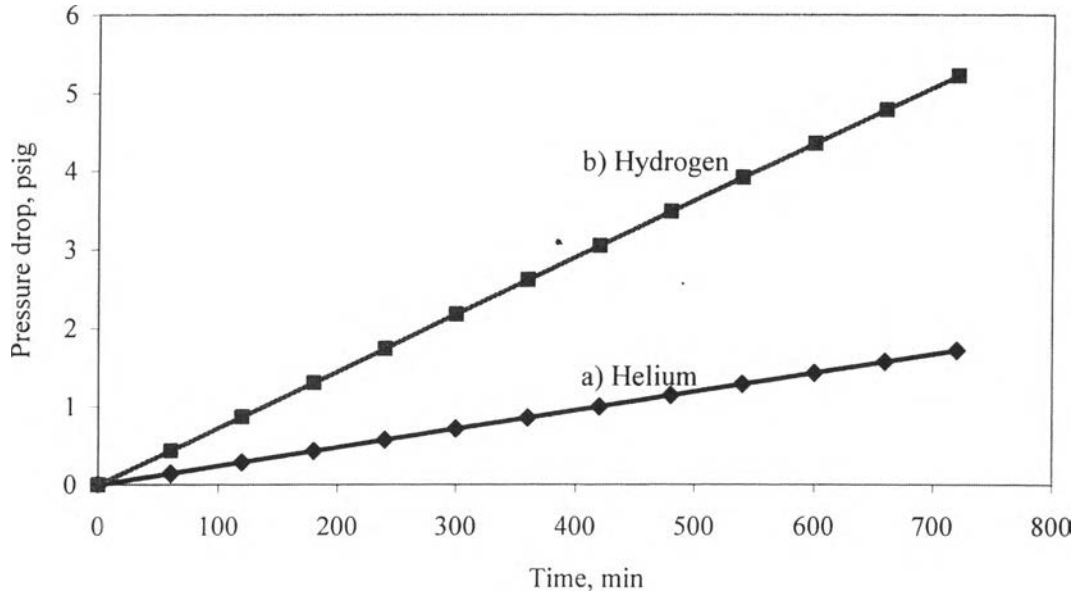

Figure 4.1 Comparison of the pressure drop during 12 hr between a) helium and b) hydrogen at 2000 psig initial pressure.

4.1.2 Volume Calibration of the Manifold and Sample Holder

Helium pressures were varied to measure the manifold volume as given in Table 4.1. And the average value of the calculated volumes of the manifold is 4.14 cm^3.

According to the multi-step experiment of helium gas (2000 psig) in the volume measurement of the sample holder, the pressure reached a constant value within 2 min after closing and helium expansion (no absorption). Pressure data in the sample holder are shown in Figure 4.2. P_1 and P_2 refer to the pressure in the manifold and sample holder, respectively. Standard deviation of the pressure is less than 0.2% conforming to the global error of the pressure transducer. By the calculation method in Appendix A, a series of estimated volume of the sample holder from Equation (3.4) in section 3.3.2.2 is given in Table 4.2. As the dead volume in the sample holder may vary depending on an amount of $NaAlH_4$, the average values of a sample holder is in the range of 17-18 cm^3.

Table 4.1 Manifold volume estimated by water displacement

Experiment no.	Pressure (psig)	Volume (cm^3)
1	100	4.06
2	200	4.14
3	300	4.15
4	400	4.13
5	500	4.16
6	1000	4.18
7	2025	4.13
8	2030	4.13
Average		4.14

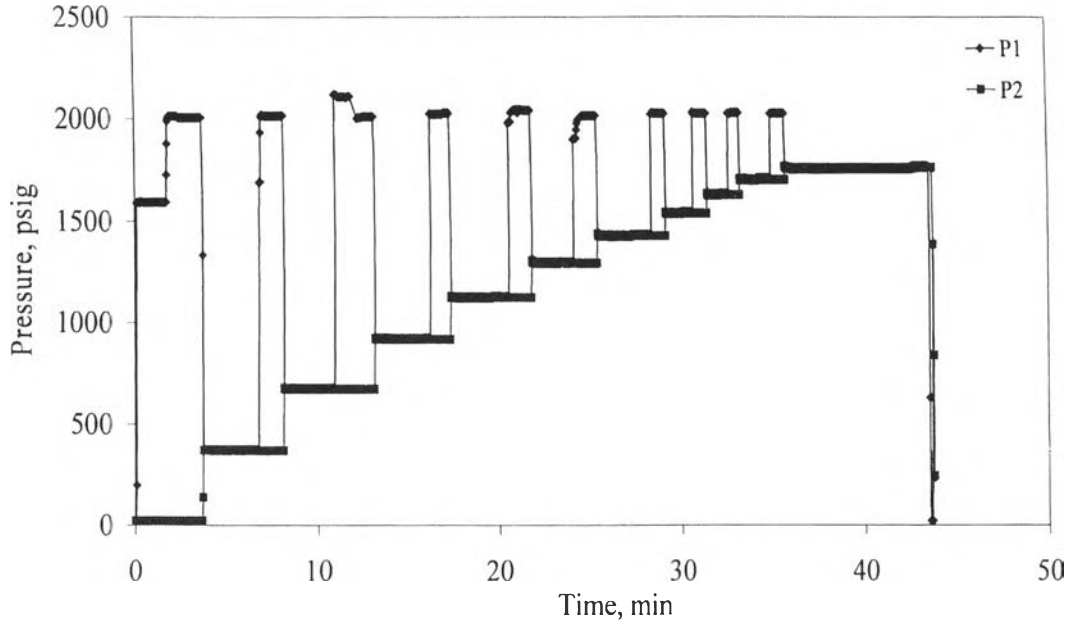

Figure 4.2 Continuous pressurization used for the estimation of the dead volume of the sample holder.

Table 4.2 Dead volume of the sample holder

Experiment no.	Initial state P_1 (psig)	Final state P_2 (psig)	V_2 (cm^3)
1	2001.5	381.7	16.97
2	1998.5	685.7	17.14
3	1997.8	932.6	17.20
4	1997.1	1134.8	17.22
5	1997.8	1299.6	17.18
6	1997.1	1432.2	17.21
7	2002.9	1542.9	17.35
8	2019.0	1634.4	17.16
9	2006.6	1705.5	17.20
10	2006.6	1764.1	17.22
Average			17.19

4.2 Hydrogen Desorption

4.2.1 Pressure Correction

By rising up the temperature, the intitial pressure of helium in the reactor was 54.7 psig at 25 °C compared to 666.3 psig at 250 °C. The remaining pressure refers to hydrogen evolved from the sample as shown in Figure 4.3.

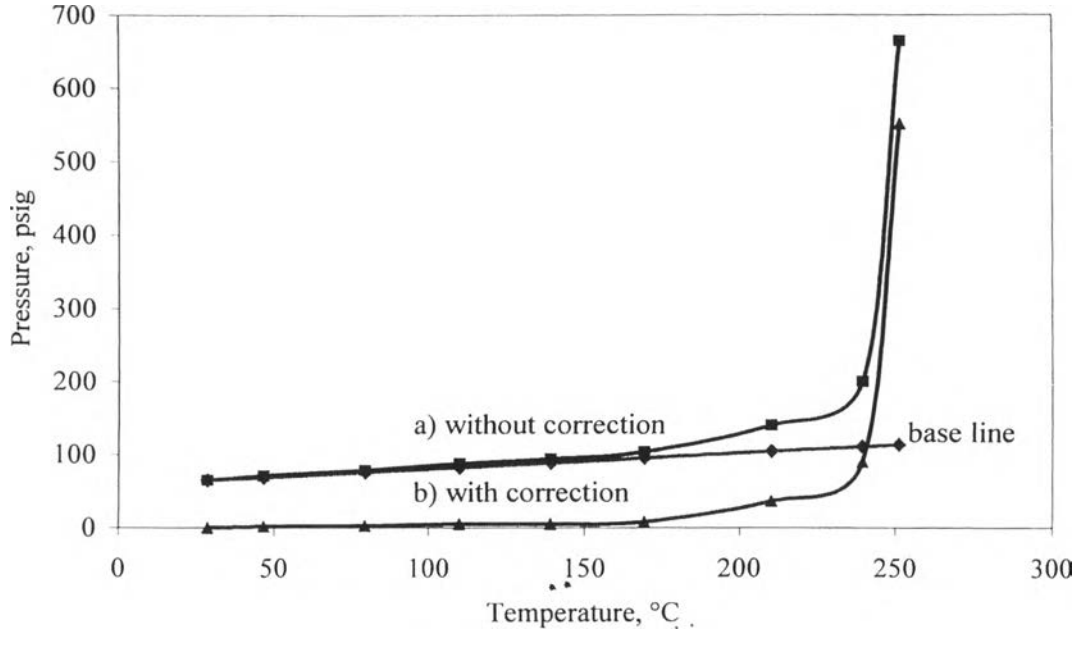

Figure 4.3 Comparison of hydrogen desorption of the purified $NaAlH_4$ before correction and after correction.

4.2.2 Effect of Purification

Since as-received $NaAlH_4$ was contaminated by aluminum, purification is needed (Zaluska *et al.*, 2000). Figure 4.4 shows the characteristics of the as-received and purified $NaAlH_4$. The purified $NaAlH_4$ is white fine powder in contrast to the as-received sample.

Plots of desorbed hydrogen weight percentage as a function of temperature are in Figure 4.5. The purified $NaAlH_4$ has higher hydrogen capacity than the as-received material, but the hydrogen desorption occurs at higher temperature than the unpurified one. This may be because the purified material

composes of mostly crystalline phases, which is difficult to decompose, or aluminum in unpurified $NaAlH_4$ activates on the hydrogen desorption by participating in the bond breaking.

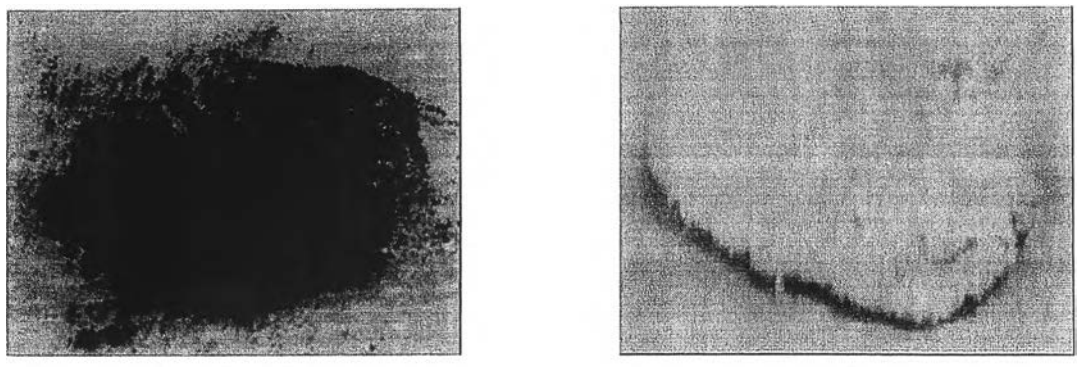

a) b)

Figure 4.4 Characteristics of a) as-received $NaAlH_4$ and b) purified $NaAlH_4$.

The obtained hydrogen capacity is less than the theoretical value (5.6 wt%) (Bogdanović *et al.*, 1997) and that reported by Jensen *et al.* (1999) as shown in Figure 4.6. This is probably due to the different technique used. Jensen *et al.* (1999) used the Schlenk technique, which can effectively control oxygen and water contamination than the dry technique used in this research. It should be noted that oxygen and water residue cause surface damage and obstruct the desorption/absorption kinetics.

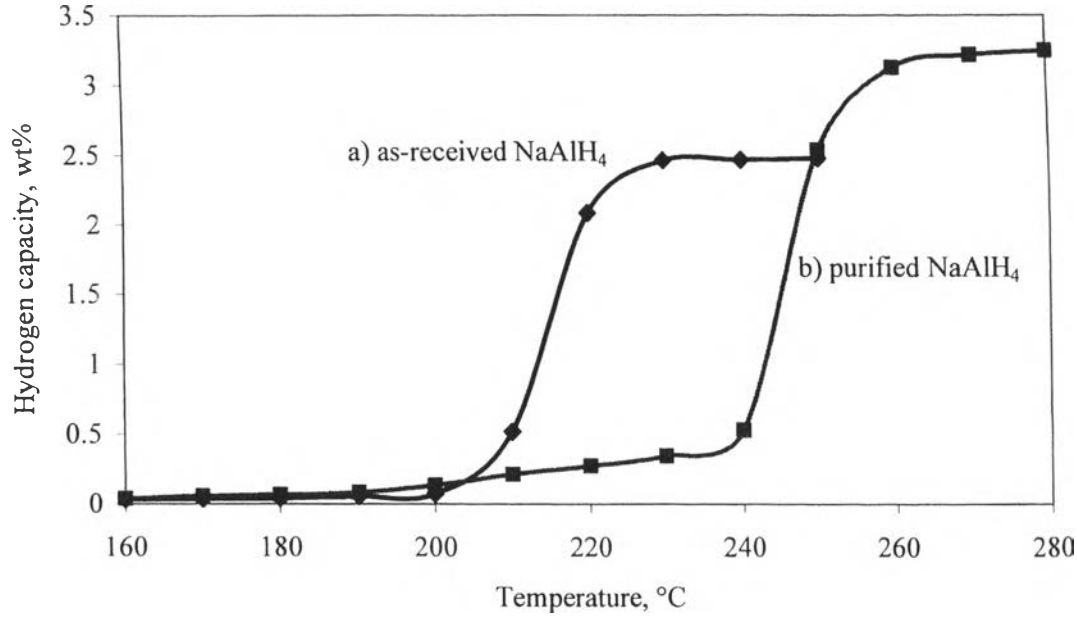

Figure 4.5 Hydrogen desorption temperature of purified and as-received $NaAlH_4$.

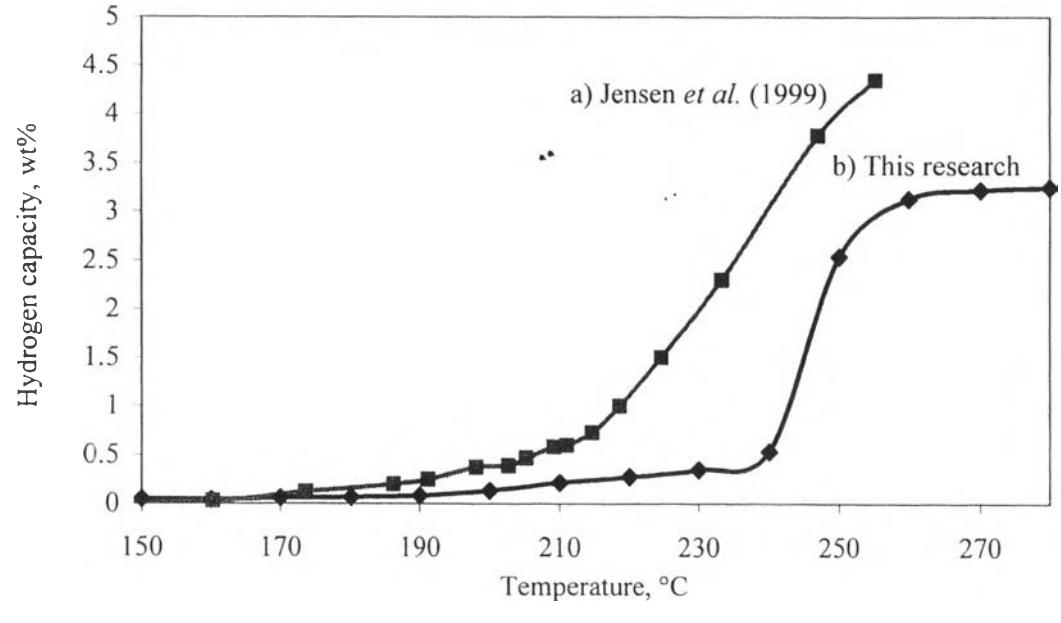

Figure 4.6 Hydrogen capacity of the purified $NaAlH_4$ as a function of temperature from this research compared with that from Jensen *et al.* (1999).

4.2.3 Effect of Metal Loading Types

With the metals in the same group from the periodic table loaded, it was discovered that different metals contribute differently to the reaction paths. Considering the decomposition reactions, Equation (2.4), hydrogen desorption from the first reaction of $NaAlH_4$ with $TiCl_3$ loaded takes place at the lowest temperature (170 °C). On the other hand, the hydrogen desorption capacity from the second decomposition of $NaAlH_4$ promoted by either $ZrCl_4$ (2.99 wt%) or $HfCl_4$ (2.8 wt%) is higher than that promoted by $TiCl_3$ (2.6 wt%). It can be inferred that $TiCl_3$ enhances the first reaction whereas $ZrCl_4$ and $HfCl_4$ do for the second reaction as illustrated in Figure 4.7.

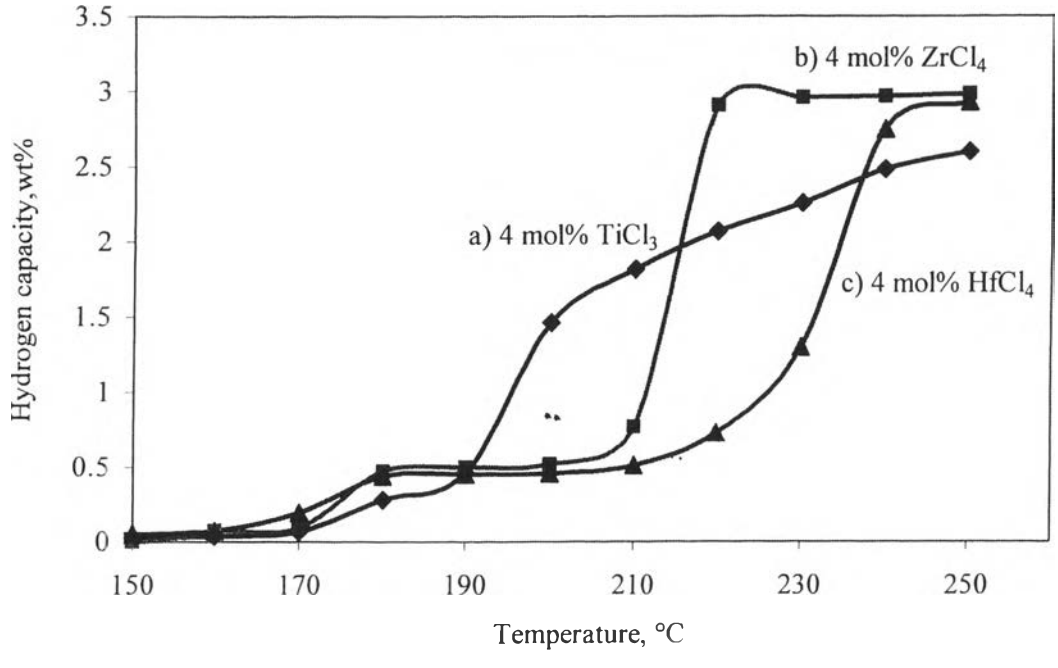

Figure 4.7 Hydrogen desorption at different temperatures of $NaAlH_4$ doped with $TiCl_3$, $ZrCl_4$, and $HfCl_4$.

4.2.4 Effect of Metal Loading Amount

In this experiment, 2, 4, 6 and 9 mol% of $ZrCl_4$ were used. The hydrogen desorption capacity is reported in Figure 4.8, the increment of hydrogen pressure in the reactor as a function of temperature. It was found that $NaAlH_4$ doped with $ZrCl_4$ results in the hydrogen desorption at lower temperature than those

without it. Only a small amount of $ZrCl_4$ can improve the hydrogen desorption rate as illustrated in Figure 4.9.

As observed in Figure 4.9, the hydrogen desorption rate does not increase any further when the amount of $ZrCl_4$ is higher than 6 mol%. It can be hypothesized that this may be caused by the lattice distortion due to the atomic substitution in formation of Zr^{2+} and Zr^{3+} instead of Zr^{4+}. It is this distortion that causes the increase in the lattice of $NaAlH_4$ so that hydrogen can absorb and desorb easily. As the amount of $ZrCl_4$ loaded reaches a certain extent, extra $ZrCl_4$ does not contribute to the lattice distortion (Dalin *et al.*, 2002).

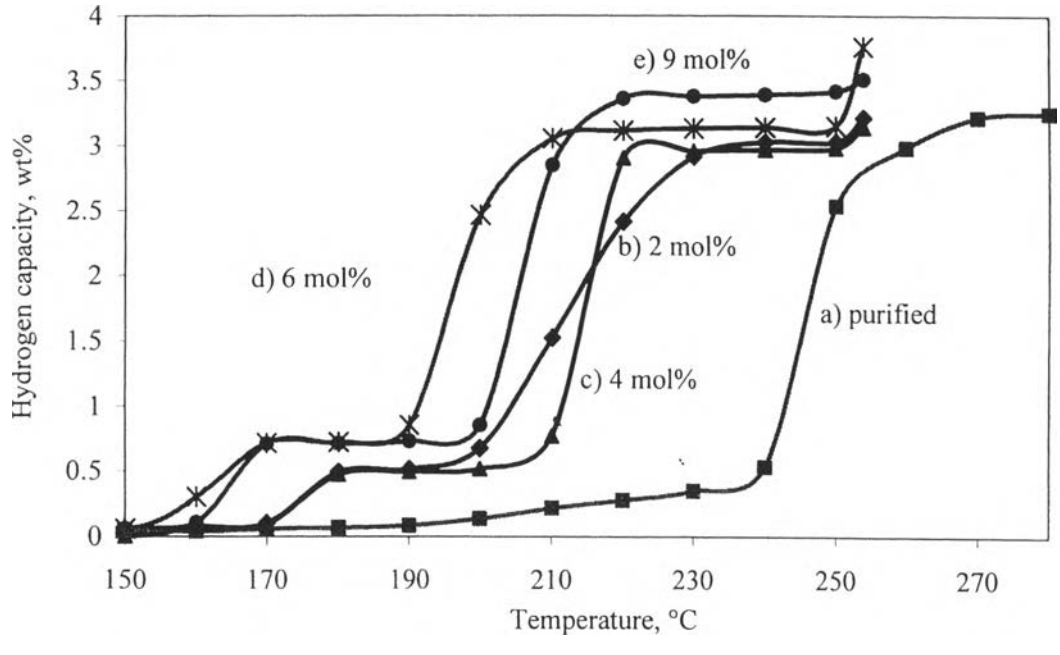

Figure 4.8 Hydrogen desorption as a function of temperature with purified and $ZrCl_4$- doped $NaAlH_4$.

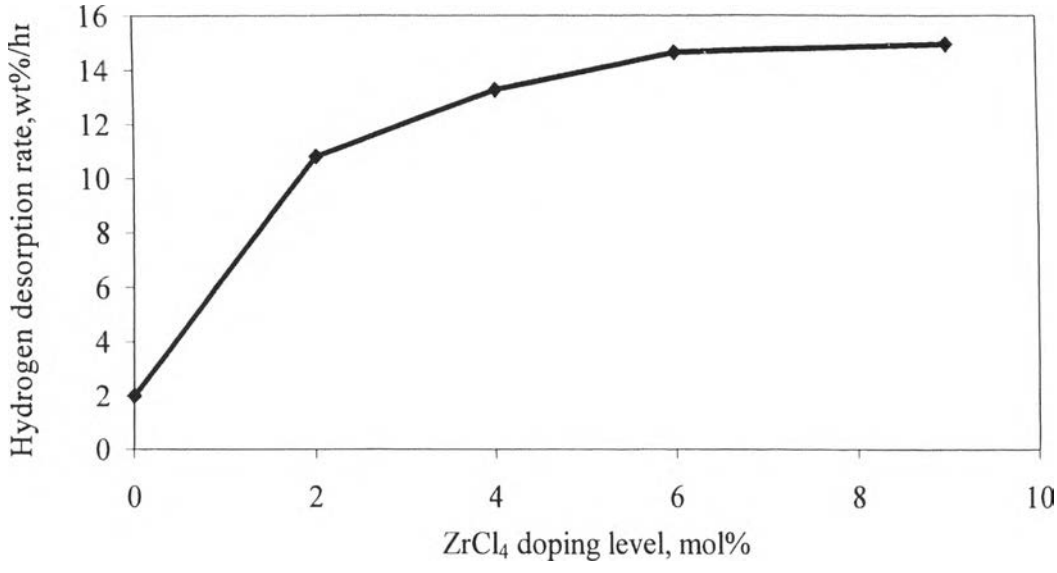

Figure 4.9 Hydrogen desorption rate as a function of doped $ZrCl_4$.

4.3 Hydrogen Absorption

4.3.1 Effect of Metal Loading Amount

Real-time absorption kinetics at 125 °C shown in Figure 4.10 represents hydrogen pressure drop as a function of time. The sample doped with 9 mol% of $ZrCl_4$ exhibits the fastest absorption kinetics in the first 40 min (Figure 4.11). The initial rate of hydrogen absorption increases proportionally with the increasing amount of $ZrCl_4$ whereas the absorption capacity shows the opposite direction as illustrated in Figure 4.12. After 12 hr, the sample doped with 9 mol% of $ZrCl_4$ reaches only 1.5 wt% H_2. This attained capacity is lower than that from the sample doped with 6 mol% of $ZrCl_4$. This leads us to establish that there is a trade-off between the kinetic performance improvement and reversible capacity exhibited in Figure 4.12. According to Gross *et al.* (2000), it is possible that NaCl forms during $NaAlH_4$ decomposition following these equations:

$$2\,NaH + \frac{1}{2}\,ZrCl_4 \rightarrow 2\,NaCl + \frac{1}{2}\,H_2 + \frac{1}{2}\,ZrH_2 \qquad (4.1)$$

$$NaH + ZrCl_4 \rightarrow NaCl + Zr + 2H_2 \qquad (4.2)$$

Because Gibb's free energy of the reaction in Equation (4.2) is lower than that of Equation (4.1), it is interpreted that NaCl is likely to come from Equation (4.2) at low $ZrCl_4$-extent and from both equations at higher level of $ZrCl_4$. The decrease in the NaH amount lowers the hydrogen capacity (Gross *et al.*, 2002).

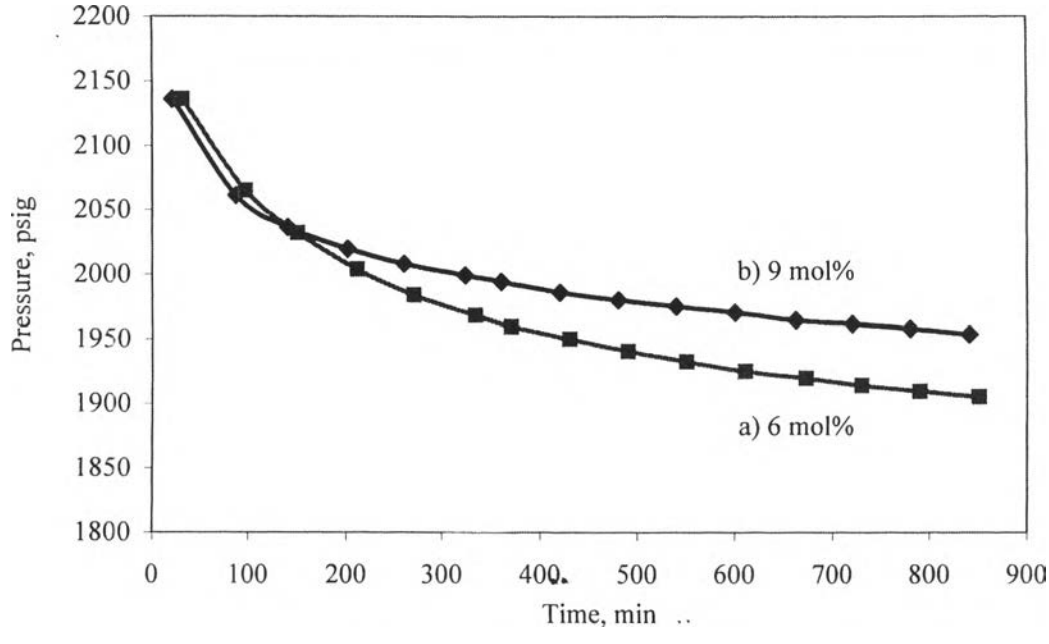

Figure 4.10 Progression of hydrogen absorptions for a) 6 mol% and b) 9 mol% of $ZrCl_4$.

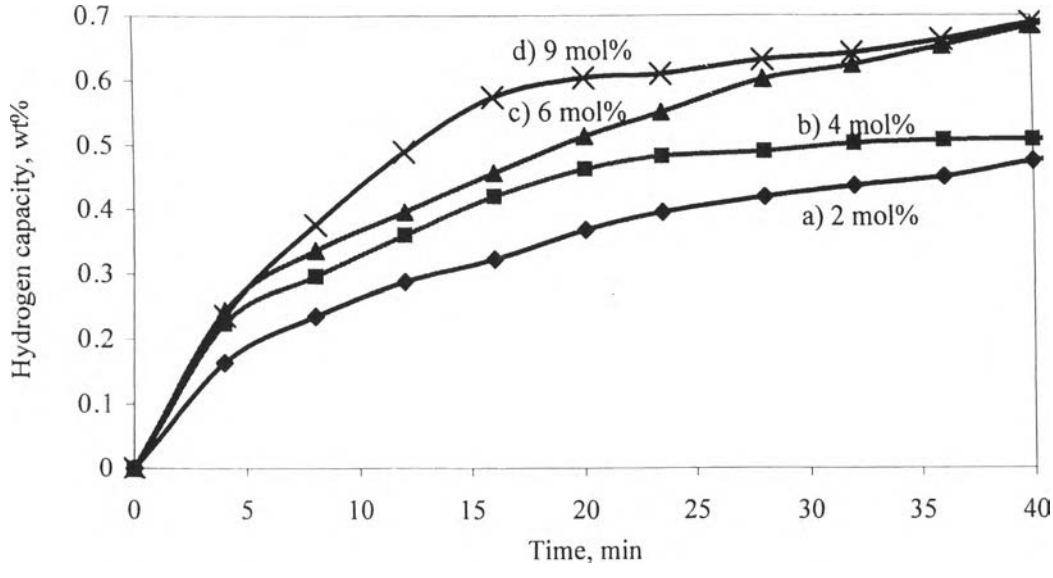

Figure 4.11 Hydrogen absorption kinetics as function of time of $NaAlH_4$ doped with 2, 4, 6, and 9 mol% $ZrCl_4$.

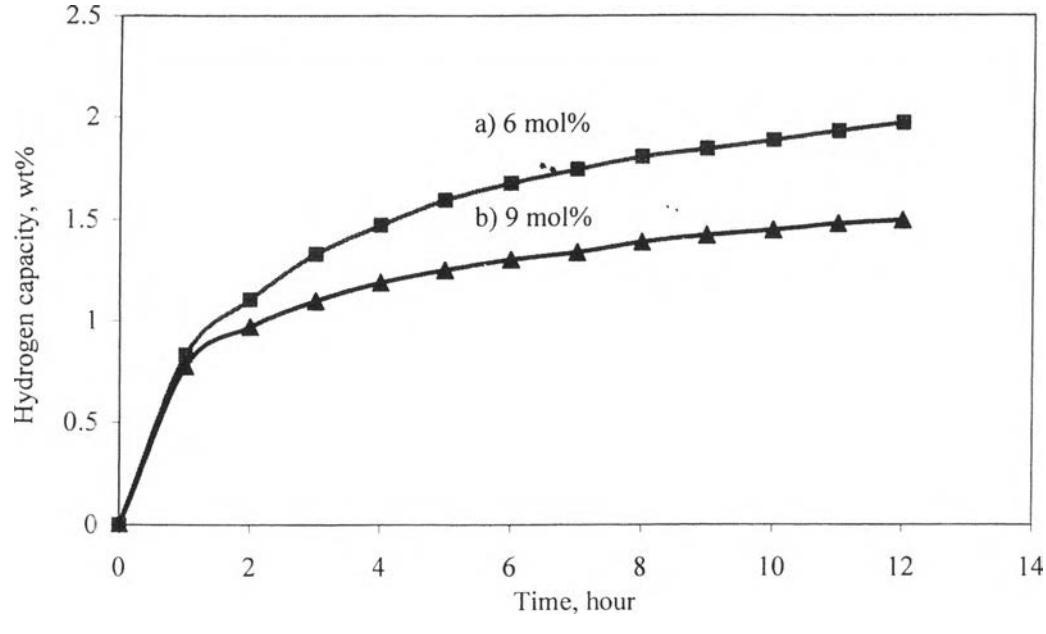

Figure 4.12 Absorption kinetics of hydrogen on $NaAlH_4$ doped with 6 mol% and 9 mol% $ZrCl_4$.

4.3.2 Effect of Metal Loading Types

The hydrogen absorption of doped $NaAlH_4$ with various halide compounds is discussed in this section. The $TiCl_3$-doped sample displays the highest hydrogen absorption rate during the 1st hour as shown in Figure 4.13. That the ionic radius plays an important role on the hydrogen absorption can be quoted (Anton, 2003). It is expected that a low rate of hydrogen discharge is observed for a doped metal with radii significantly larger or smaller than 0.74 Å, the midpoint between Na^+ (0.97 Å) and Al^{3+} (0.51 Å). Since Ti^{3+} (0.76 Å) has an ionic radius closer to the midpoint than that of Zr^{4+} (0.86 Å) and Hf^{4+} (0.85 Å) (Shannon, 1976), the $TiCl_3$-doped sample shows the highest capability for the enhancement of the hydrogen charge.

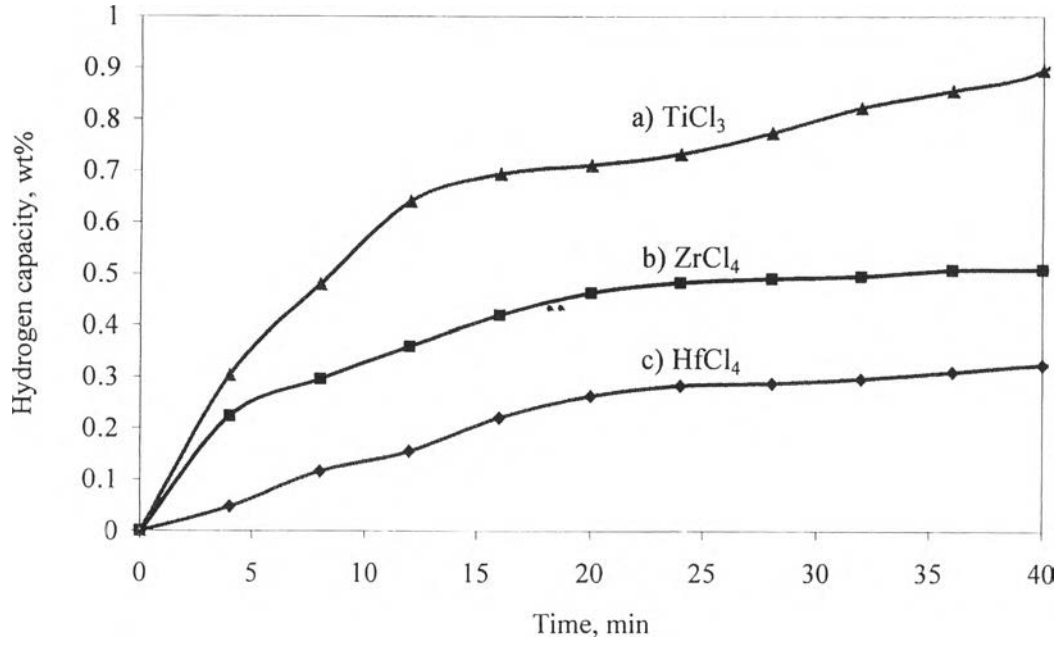

Figure 4.13 Hydrogen absorption kinetics of $NaAlH_4$ doped with $TiCl_3$ (4 mol%), $ZrCl_4$ (4 mol%), and $HfCl_4$ (4 mol%).

A reason why hydrogen uptake rate of $HfCl_4$-doped material is lower than that of the $ZrCl_4$-doped one is possibly concerned with symmetry of orbitals. Among the three species, Hf^{4+} has an electron configuration in the f orbital whereas

that of others are in p orbital, synchronizing with Al^{3+}. So, this configuration is quite tough to cause atomic overlap between Al^{3+} and Hf^{4+}. The sample rendered by $ZrCl_4$ sustains hydrogen at higher capacity so it can be interpreted that the activity of $HfCl_4$ as a catalyst is considerably lower than that of $ZrCl_4$.

This result leads to conclude that $HfCl_4$ has less ability to reverse $NaAlH_4$ decomposition than $ZrCl_4$. The recycle ability is called the degree of rehydrogenation (Bogdanovic *et al.*, 2000), a portion of absorption and desorption capacity. Nevertheless, all of the doped samples are not entirely reversible, which generally shows lower absorption capacity than the desorption capacity, Table 4.3. A major reason might be the incomplete absorption owing to the forming of large metallic aluminum particles hampers the mass transfer problem (Bogdanovic *et al.*, 2003).

Table 4.3 Total hydrogen capacities measured by absorption and desorption procedure, including the estimated degree of rehydrogenation at different types of doped metals

Hydrogen capacities(wt%)*			Degree of rehydrogenation (%)
Type of metal loadings	Desorption	Absorption	
$TiCl_3$	3.05	1.93	63.3
$ZrCl_4$	3.14	1.78	56.7
$HfCl_4$	2.88	1.42	49.3

* These values were reported at 4 mol% of doped metal.